Digital Discovery

ROYAL SOCIETY OF CHEMISTRY

PAPER

View Article Online
View Journal | View Issue

Cite this: *Digital Discovery*, 2026, **5**, 862

A data-driven approach to control stimulus responsivity of functional polymer materials: predicting thermoresponsive color-changing properties of polydiacetylene

Risako Shibata,[a] Nano Shioda,[a] Hiroaki Imai,[a] Yasuhiko Igarashi[bc] and Yuya Oaki*[a]

Sensing devices are fabricated using stimuli-responsive materials. In general, the responsivity is controlled by designing molecules and materials based on professional experience. If predictors are constructed for the responsivity control, the number of experiments can be reduced without consumption of time, cost, and effort. However, such dynamic properties of functional polymer materials are not easily predicted because of the small data and complex structure–function relationship. How to prepare a dataset and train small data remain significant challenges. The present work shows construction and application of a prediction model for controlling thermoresponsive color-changing properties of layered polydiacetylenes (PDAs). The responsivity was changed by the intercalated guest molecules. The training dataset was prepared from a series of the photographs representing the color at each temperature. The prediction model of the thermoresponsivity, namely color-changing temperature, was constructed by combining machine learning and our chemical insight based on the small experimental data. The thermoresponsivity of the newly synthesized layered PDAs was predicted by the model. The modeling methods can be applied to predict various dynamic properties of functional polymer materials.

Received 1st October 2025
Accepted 3rd January 2026

DOI: 10.1039/d5dd00442j

rsc.li/digitaldiscovery

1. Introduction

Stimuli-responsive molecules and materials have various applications, such as sensors and actuators.[1–11] An input external stimulus, such as thermal, chemical, optical, and mechanical stimuli, is converted to a specific output response by molecules and materials. Visible and/or fluorescent colors are used for detection of the applied stresses. The responsivity, such as sensitivity, chromaticity, and reversibility, is tuned by design and synthesis of chromophores and their organization states. In general, such molecules and materials are designed based on professional experiences and synthesized with trial and error. If a data-driven approach is effectively applied to these processes, the responsivity can be efficiently tuned without consumption of time, cost, and effort. Although this motivation is rational, data-driven approaches are not easily applied for designing such functional soft materials because of the following reasons. One of the problems is the insufficient data size of typical experimental procedures for the use of conventional machine-learning (ML) algorithms. Another problem is how to prepare a dataset suitable for ML based on non-numerical experimental results. The targeted problem, *i.e.* stimuli responsivity, should be translated into a ML-solvable problem. For example, photographs, spectra, and their changes need to be converted to ML-applicable data. Moreover, as dynamic properties are related to the complex structural hierarchy ranging from molecules to organized states, the factors related to the properties as the potential descriptors are not fully prepared only using conventional tools for automatic generation of descriptors. In this manner, ML has not been fully applied to experimental studies for controlling the properties of stimuli-responsive materials because of the issues in data size, data curation for the targets, and preparation of the descriptors. Although ML has been applied to design polymers and soft materials, such as polymers, gels, liquid crystals, and bubbles, in recent years,[12–22] further methodological advances are required to develop the methods for small experimental data. The present work shows construction of a prediction model for thermoresponsive color-changing properties of layered PDAs (Fig. 1). Based on the photographic data, a straightforward linear regression model was prepared by sparse modeling for small data (SpM-S). The data acquisition, curation, and modeling methods can be applied to construct the predictors of

[a]*Department of Applied Chemistry, Faculty of Science and Technology, Keio University, 3-14-1 Hiyoshi, Kohoku-ku, Yokohama 223-8522, Japan. E-mail: oakiyuya@applc.keio.ac.jp*

[b]*Institute of Engineering, Information and Systems, University of Tsukuba, 1-1-1 Tennodai, Tsukuba 305-8573, Japan*

[c]*Tsukuba Institute for Advanced Research (TIAR), University of Tsukuba, 1-1-1 Tennodai, Tsukuba, 305-8577, Japan*

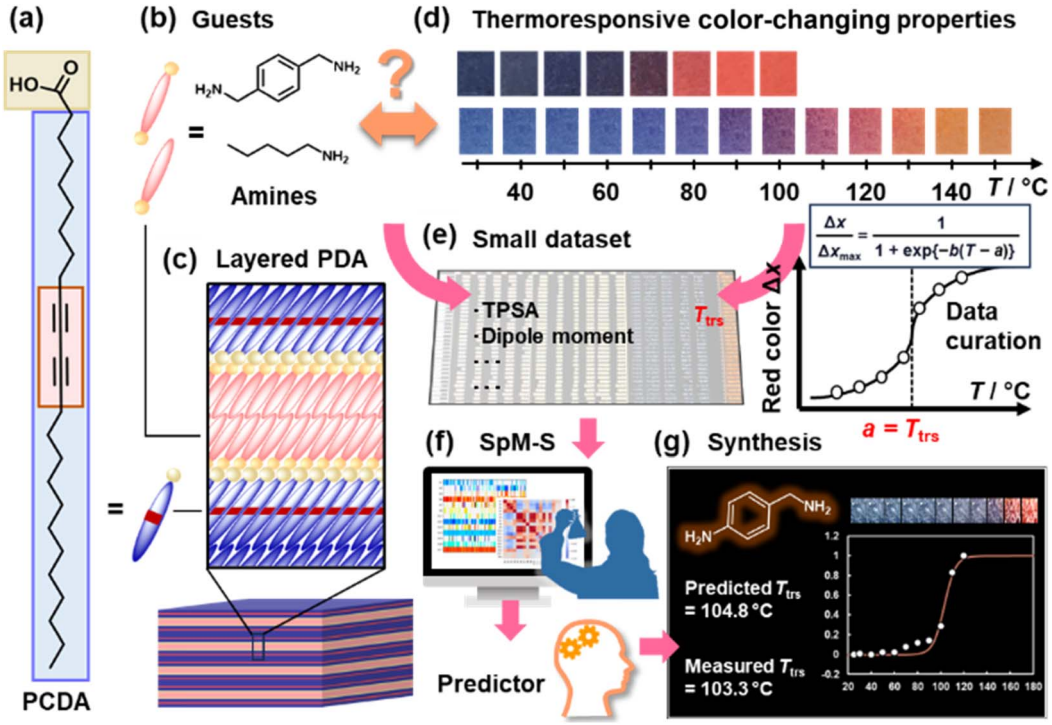

Fig. 1 Schematic illustration for predicting thermoresponsive color-changing properties of layered PDAs. (a) PCDA monomer. (b) Guest amines. (c) Guest-intercalated layered PDA with topochemical polymerization. (d) Photographs for preparing thermoresponsive color-changing properties. (e) Small dataset containing the color transition temperature ($T_{trs} = y$, objective variables) and physicochemical parameters of the guests (x_{Gn}, explanatory variables). (f) SpM-S for extraction of the descriptors and model construction. (g) Synthesis of the layered PDA with intercalating new guests based on the predicted T_{trs}.

the other stimuli-responsive functional materials with small data.

PDA, a conjugated polymer, exhibits color changes in response to external stimuli, such as thermal, chemical, and frictional stresses.[23–30] A wide variety of sensing devices and systems were fabricated using PDA. The stresses induce molecular motion and subsequent shortening of the effective conjugation length of the PDA main chain. The stimuli responsivity has been controlled by the molecular design.[31–43] Our group has studied an intercalation approach to control the responsivity of layered PDAs (Fig. 1a–d).[45–52] The layered structure of an amphiphilic diacetylene (DA) monomer, 10,12-pentacosadiynoic acid (PCDA), is topochemically polymerized in the solid crystalline state (Fig. 1a and c). Whereas the layered PDA derived from PCDA shows the blue-to-red color transition around 65 °C with heating (Fig. 1d), the color-changing temperature varied in the range from −0.2 to 146 °C depending on the intercalated guests, such as metal ions and alkyl amines, in the interlayer space (Fig. 1b and d).[44–52] However, responsivity control based on experience and intuition meets the limitations for both the molecular-design and intercalation approaches. Here we used ML to construct the predictor for controlling the responsivity.

In recent years, ML has been widely used in general materials science.[53–60] Most of the algorithms are suitable for big data. A sufficient size of data is not available for all the experimental works. With small data, conventional ML algorithms cause problems, such as overtraining. Recent studies have proposed specific methods for small data, such as transfer and active learning.[61–67] In our group, sparse modeling for small data (SpM-S) has been studied; the approach combining ML and our chemical insight provides straightforward and interpretable predictors.[68–73] SpM-S was used for simple numerical data, such as yield, size, and capacity, directly obtained from the experimental procedures. The approach was not applied to small experimental data requiring curation prior to use, such as photographs and graphs. If the targeted data and problem are converted to SpM-S applicable formats in an appropriate manner, the approach can be applied to small data in broader fields. In the present work, a prediction model for the thermoresponsive color-changing properties of the layered PDA was constructed by SpM-S (Fig. 1d–g). After the training dataset was prepared from a series of photographic data (Fig. 1d and e), combination of ML and chemical insight provides predictors based on the small data (Fig. 1f). The model successfully predicted the thermoresponsivity of the layered PDAs with the intercalation of new unknown guests (Fig. 1g). Based on these results, if the targeted stimuli responsivity is converted to an appropriate dataset, the predictors can be constructed by SpM-S even on small experimental data.

2. Results and discussion

2.1. Preparation of datasets from photographs

The data about the thermoresponsive color-changing properties were extracted from our previous studies and newly added in

the present work (Fig. 1b–d, S1–S3 and Tables S1–S3 in the (SI)).[44–51] The layered PDAs show color changes from blue to red with increasing temperature (T/°C) (Fig. 1d). Whereas the layered PDA without the guest showed a blue-to-red color transition around 65 °C, for example, the color transition was observed around 80 and 100 °C with the intercalation of tetradecylamine (C_{14}-NH_2) and *p*-xylylenediamine (*p*-Xy), respectively (Fig. 2a and b).

The original experimental data are a series of photographs exhibiting the color of the sample at different temperatures. The color of the photographs was converted to the red-color intensity (x) based on the RGB values using an international standard (see the Experimental Method in the SI). An increment of x ($\Delta x = x - x_0$) was calculated at each T in reference to the initial state before heating (x_0). Then, Δx was normalized by dividing it by the maximum Δx_{max} ($\Delta x/\Delta x_{max}$). The relationship between T and $\Delta x/\Delta x_{max}$ was prepared for each layered PDA containing 75 different guests (Fig. 2c, d and S3 in the SI). The T–($\Delta x/\Delta x_{max}$) curve was approximated using a sigmoidal function eqn (1), using two constants a and b with the coefficient of determination (R^2).

$$\frac{\Delta x}{\Delta x_{max}} = \frac{1}{1 + \exp\{-b(T - a)\}} \quad (1)$$

In the curve, the constant a corresponds to the color-changing temperature reaching $0.5\Delta x/\Delta x_{max}$ (Fig. 1e). The constant b corresponds to the slope representing the temperature responsivity. The observed T–Δx plots were approximated using eqn (1) by optimizing a and b to minimize the R^2 value. The average R^2 values were 0.952 ± 0.066 for all the data (Table S4 in the SI). The fitting function was prepared with the specific a and b for each sample (Fig. 2c, d and S3 in the SI). The color-transition temperature (T_{trs}) was defined as the T at which $0.5\Delta x/\Delta x_{max}$ is reached, namely a in eqn (1). The sigmoidal function is a suitable approximation to describe the temperature-responsive chromaticity change. A sigmoidal function generally exhibits the following trend of increase in y: gentle increases in the initial and final stages and a steep increase in the middle range. The same trend was experimentally observed for the thermoresponsive color-changing behavior of PDAs (Fig. 2c and d). As the variation of the chromaticity change, $\Delta x/\Delta x_{max}$, is limited in a specific range, this behavior is also represented by the sigmoidal function. In this manner, the thermoresponsive color-changing properties based on a series of photographs were converted to numerical data.

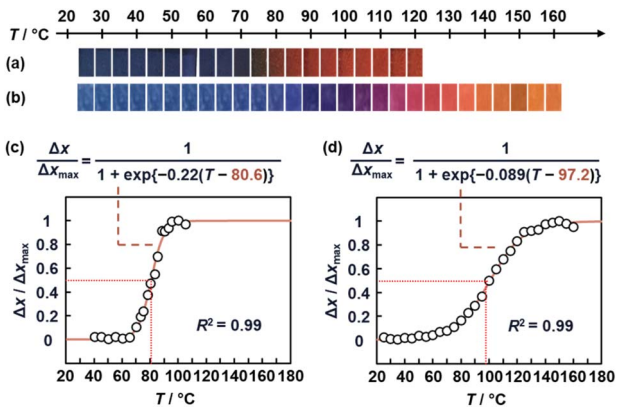

Fig. 2 Data curation of the thermoresponsive color-changing properties. (a and b) Photographs representing the relationship between T and color of layered PDAs with the intercalation of C_{14}-NH_2 (a) and *p*-Xy (b). (c and d) Approximation of the relationship between T and $\Delta x/\Delta x_{max}$ (each plot) generated from the photographic data using a sigmoidal function (red curve) for PDA-C_{14}-NH_2 (c) and PDA-*p*-Xy (d). The same data for the other amines are summarized in Fig. S3 in the SI.

Table 1 List of explanatory variables

x_{Gn}	Parameter	Unit	[a]Method
x_{G1}	HSP dispersion	$MPa^{1/2}$	H
x_{G2}	HSP polarity	$MPa^{1/2}$	H
x_{G3}	HSP hydrogen bonding	$MPa^{1/2}$	H
x_{G4}	Density	g cm^{-3}	H
x_{G5}	Molecular volume	cm^3 mol^{-1}	H
x_{G6}	Molecular surface area	cm^2 mol^{-1}	H
x_{G7}	Boiling point (1.01×10^5 Pa)	°C	H
x_{G8}	Melting point (1.01×10^5 Pa)	°C	H
x_{G9}	Ovality	—	H
x_{G10}	Molecular weight	g mol^{-1}	R
x_{G11}	[b]Log P	—	R
x_{G12}	[c]TPSA	$(10^{-10}$ m$)^2$	R
x_{G13}	Molecular length	10^{-10} m	R
x_{G14}	Minimum of partial charge density	C m^{-3}	G
x_{G15}	Polarizability	$(10^{-10}$ m$)^3$	G
x_{G16}	Dipole moment	Debye	G
x_{G17}	Valence of amine	—	—

[a] Softwares: HSP-ip (H), RDKit (R), Gaussian (G) (See the SI). [b] Logarithm of partition coefficient between water and octanol. [c] Topological polar surface area.

2.2. Construction of the T_{trs} predictor

The original 75 data points were divided into the training and test datasets containing 65 y and 10 y, respectively (Tables S2 and S3 in the SI). The variable selection was carried out using the training dataset (Fig. 3 and Table S2 in the SI). As the correlation coefficients of x_{Gn} (n = 5, 6, 9, 10) were larger than 0.9 (Fig. S4 in the SI), these four x_{Gn} were removed to avoid multicollinearity. In SpM-S,[68] the significance of x_{Gn} was visualized in the weight diagram of exhaustive search with linear regression (ES-LiR) (Fig. 3a).[69,73] Linear regression models were prepared using the training dataset in all the possible combinations of 13 x_{Gn} (n = 1–4, 7, 8, 11–17), 2^{13}–1 (=8.2 × 10^3) combinations, with five-fold cross validation (CV). The constructed models were sorted in the ascending order of the cross-validation error (CVE) values. The positive and negative

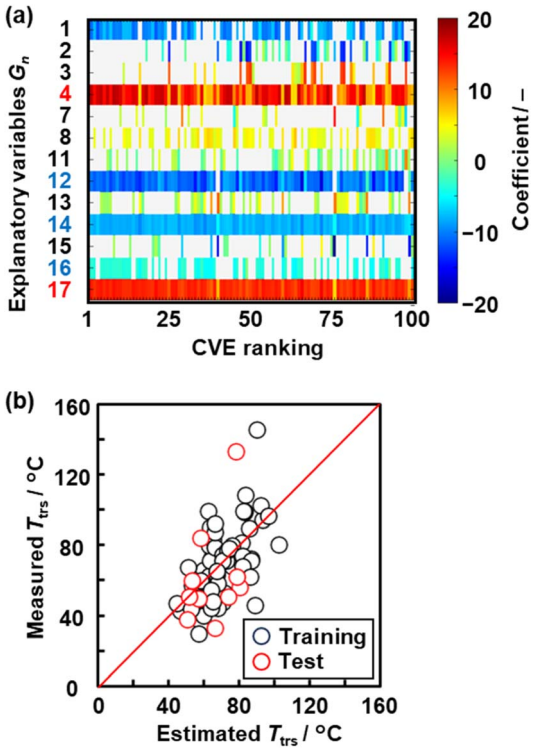

Fig. 3 Construction of the T_{trs} prediction model. (a) Weight diagram of ES-LiR. (b) Relationship between the estimated and measured T_{trs} for the training (black, 65 *y*) and test (red, 10 *y*) datasets using the model eqn (2) composed of five x_{Gn} (x_{G4}, x_{G12}, x_{G14}, x_{G16}, and x_{G17}), respectively.

coefficients of x_{Gn} were represented by the warm and cool colors in the diagram, respectively (Fig. 3a). The more frequently used x_{Gn} was displayed by the more densely colored bar on the vertical axis. Based on the weight diagram, we selected five x_{Gn} (x_{G4}, x_{G12}, x_{G14}, x_{G16}, and x_{G17}) as the descriptors to prepare the linear regression model eqn (2).

$$y = 8.85x_{G4} - 6.66x_{G12} - 7.38x_{G14} - 5.76x_{G16} + 12.04x_{G17} + 68.67 \quad (2)$$

As the coefficients of this linear regression are normalized in frequency distribution with a mean of 0 and a standard deviation of 1, the contribution of each x_{Gn} is comparable. The relationship between the estimated and measured T_{trs} had a root mean squared error (RMSE) of 15.9 °C for the training dataset (65 *y*, black circles) and 25.3 °C for the test dataset (10 *y*, red circles) (Fig. 3b). The coefficient of determination (R^2) was 0.388 for the training dataset and 0.139 for the test dataset. Five-fold CV was carried out using the merged dataset of the training and test ones (75 *y*) (Fig. S5 in the SI). In the five-fold CV, the regression equations had the same positive and negative coefficients as those in eqn (2). RMSE was 15.6 ± 1.2 °C for the training data and 17.3 ± 4.1 °C for the test data. The RMSE values in the five-fold CV imply that the model eqn (2) is not overtrained in the training dataset but generalizable. The RMSE and R^2 values are not so high to predict T_{trs} precisely. On the other hand, the relationship between the estimated and predicted values in Fig. 3b indicates that the overall trends of the higher and lower T_{trs} are roughly described by the model. In general, a model with high prediction accuracy (*e.g.* RMSE and R^2 values) is not easily constructed based on small data because of the lack of data size. In addition to these quantitative metrics, whether the overall trend is described by the model or not is qualitatively evaluated by the plots representing the relationship between the estimated and predicted values.[68,69] If the model describing the overall trend is constructed based on small data, the next experiments can be accelerated by reducing the number of trials. In this manner, a linear regression model for predicting T_{trs} of the layered PDA was constructed by SpM-S.

The contribution of each descriptor to T_{trs} was studied based on the positive and negative values of the coefficients with our chemical insight. Density (x_{G4}) and valence (x_{G17}) of the guests have a positive correlation with T_{trs}. If the guest molecule with the higher density (larger x_{G4}) is intercalated in the interlayer space, the more densely packed guests can provide a rigid layered structure. The divalent guest amines also form the rigid layered structure by anchoring the layers at both the terminals. The

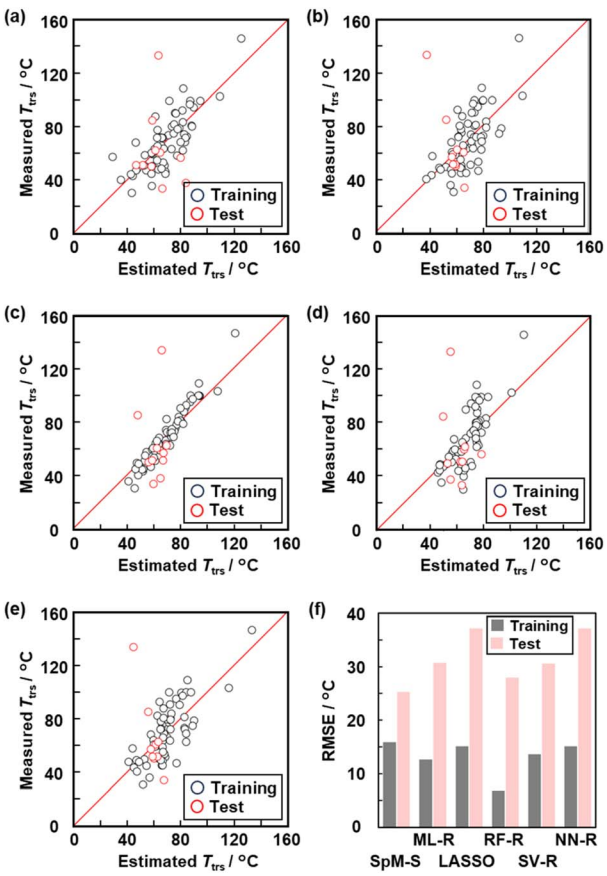

Fig. 4 Model construction using other ML algorithms. (a–e) Relationship between the estimated and measured T_{trs} for the training dataset (black, 65 *y*) and test dataset (red, 10 *y*) for ML-R (a), LASSO (b), RF-R (c), SV-R (d), and NN-R (e), respectively. (f) RMSE values of the constructed models for the training (gray) and test (pink) datasets.

minimum value of the partial charge density (x_{G14}) shows a negative correlation. The guests with heteroatoms in the alkyl chain or aromatic ring, such as secondary amines and pyridine rings, have larger x_{G14} values compared with the other primary amines (Tables S2 and S3 in the SI). These guest molecules direct formation of soft layered structures with the weakened interlayer interaction leading to a decrease in T_{trs} because of the loose packing. Topological polar surface area (TPSA, x_{G4}) and dipole moment (x_{G16}) have a negative correlation with T_{trs}. As the guest molecules with smaller x_{G4} and x_{G16} are organized and packed in the interlayer space with van der Waals interactions, an increase in T_{trs} is attributed to the more rigid layered structure. In this manner, the contribution of each x_{Gn} can be interpreted by our experience and chemical insight. In the present study, the guest monoamines and diamines with alkyl chains, cycloalkanes, aromatic and heteroaromatic rings, and alcohols were mainly used for the training (Table S1 in the SI). The other amines, such as those containing branched alkyl chains and ethers, were not fully trained in the present model. In addition, more different types, such as amino acids, macromolecules, and polyamines, need to be trained by adding more data. A more accurate model can be constructed by adding more data.

2.3. Model construction using other ML algorithms

The model construction was carried out based on the same training and test datasets using the following other linear and nonlinear ML algorithms (Fig. 4): multiple linear regression (MLR) without variable selection, least absolute shrinkage and selection operator (LASSO), random forest regression (RF-R), support vector regression (SV-R), and neural network regression (NN-R). Whereas the relationship between the estimated and observed T_{trs} approached the diagonal line for the training dataset, a large error was found for the test dataset (Fig. 4a–e). Fig. 4f summarizes the RMSE values for the original training and test datasets. The other algorithms provide slightly smaller RMSE values for the training dataset compared with that of the model constructed by SpM-S. In contrast, the larger RMSE values were obtained for the test dataset. In the case of LASSO, a larger number of the descriptors x_n (2, 5–8, 10, 12, 13, and 15) was used for the model. These results imply that the other algorithms lead to the overfitting of the training dataset and lower the generalizability to the test dataset. Similar results were obtained in our previous studies using small data.[69,70,74,75] SpM-S provides an accurate model comparable to other models

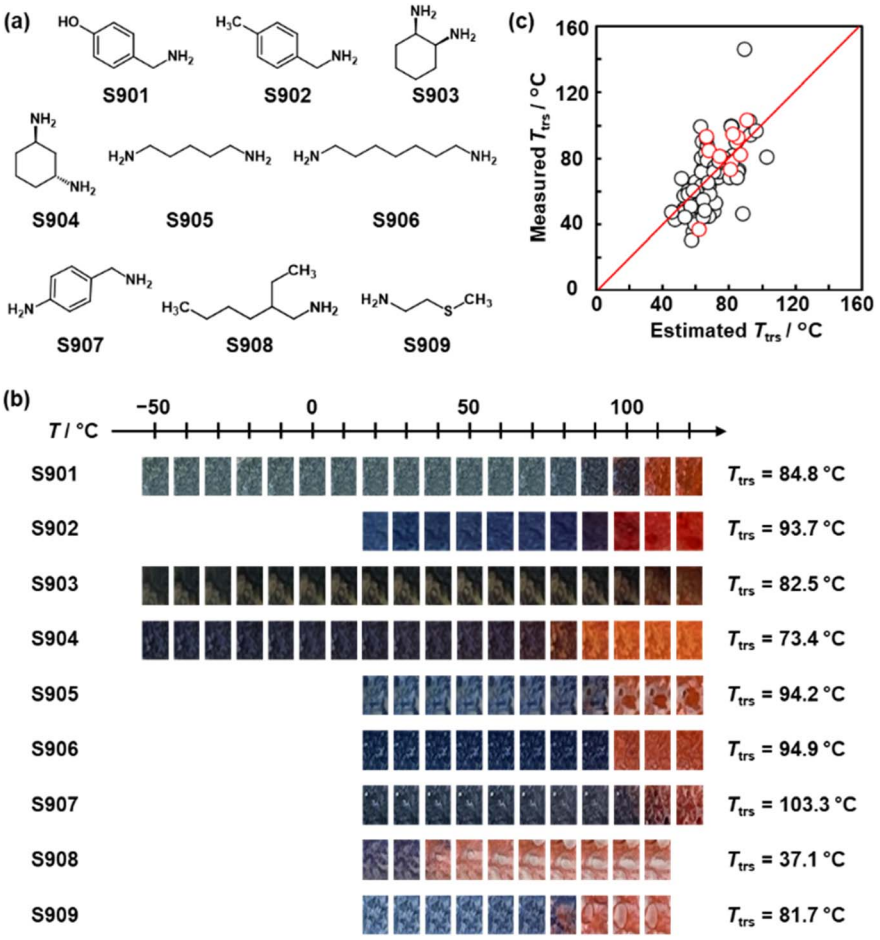

Fig. 5 Prediction-based synthesis of the layered PDA with the intercalation of new guests. (a) Molecular structure of new guests **S901–S909**. (b) Photographs representing the relationship between T and color of the layered PDA with the intercalation of the new guests **S901–S909**. The measured T_{trs} was noted with the photographs. (c) Relationship between the estimated and measured T_{trs} for the training dataset (black, 65 y) and newly synthesized ones (red, 9 y), respectively.

even though the number of the selected descriptors is limited. The linear regression model comprising the selected descriptors and coefficients has interpretability and straightforwardness. The smallest RMSE value for the test dataset indicates generalizability to unknown test data. In this manner, SpM-S is a suitable approach to small data in terms of accuracy, interpretability, and generalizability.

2.4. Prediction-based syntheses of new layered PDAs

Nine commercial amines (**S901–S909**) were selected as the new guests (Fig. 5a and Table S5 in the SI). These molecules were not used in the previous studies and datasets for the model construction. Prior to the experiments, the predicted T_{trs} was calculated using the model eqn (2). These guest-intercalated precursor layered crystals were synthesized by self-organization from a solution containing the host PCDA and guest amine with the evaporation of the solvent.[45] The layered PDA with the intercalated guests was obtained by UV-light irradiation. The intercalated structures were analyzed by X-ray diffraction (XRD) and Fourier-transform infrared (FT-IR) spectroscopy (Fig. S6 in the SI). The thermoresponsive color-changing properties were observed by heating the samples (Fig. 5b). The actual T_{trs} was calculated from the T–($\Delta x/\Delta x_{max}$) relationship by approximation using eqn (1) (Fig. S7 in the SI). The predicted and actual T_{trs} values are summarized using the red circles in Fig. 5c. The RMSE value of the actual T_{trs} was 15.6 °C comparable to that of the training data (15.9 °C, black circles in Fig. 5c). The results indicate that T_{trs} of the guest-intercalated layered PDA can be predicted using the model. Although the guests have been selected based on our experience and intuition, a more efficient selection can be achieved using the predictor in the future. Moreover, a similar approach can be applied to the molecular design of DA monomers to achieve tailored responsivity.

3. Conclusions

A dynamic function of polymer materials has been predicted based on small experimental data with the assistance of ML, SpM-S. Layered PDAs show thermoresponsive color-changing properties depending on the intercalated guest molecules. As the color-changing properties were represented by a series of photographs in our experimental studies, the ML-applicable data were prepared at the initial data-curation step. The relationship between T and $\Delta x/\Delta x_{max}$ representing the thermoresponsivity was approximated using a sigmoidal function for conversion of the photographic data to numerical data for ML. A constant in the fitting function was set as y. The descriptors were extracted from the weight diagram representing the contribution of each x_n. The straightforward and interpretable linear model was constructed for predicting T_{trs} by SpM-S. Furthermore, T_{trs} of the layered PDA with intercalation of the new guest was predicted prior to the experiment. The actual T_{trs} was consistent with the predicted one. These results indicate the successful construction of the T_{trs} predictor for layered PDAs. In general, dynamic functions of polymer materials are not easily predicted because of the complex structural hierarchy. The present approach combining data curation and SpM-S can be applied to other stimuli-responsive materials with input triggers (*e.g.* temperature, concentration, pH, and light) and output signals (*e.g.* color change, phase and structural transitions, morphology change, and current). Moreover, designing other functional polymer materials can be achieved using the present method based on small data.

Conflicts of interest

There are no conflicts to declare.

Data availability

The data supporting this article have been included as part of the supplementary information (SI). The following datasets are available at GitHub of our group (https://github.com/Oaki-Group/202511_PDA) (DOI: https://doi.org/10.5281/zenodo.18060256): Tables S1 and S5 as a csv file with simplified molecular input line entry system (SMILES) and mol2 files; Table S2 as a csv file for the training dataset; Table S3 as a csv file for the test dataset. The following codes are available at the above website: ES-LiR; drawing weight diagram; the other ML algorithms as the reference. Supplementary information: experimental methods, list of guest molecules, datasets, XRD patterns, FT-IR spectra, and thermoresponsive color-changing properties. See DOI: https://doi.org/10.1039/d5dd00442j.

Acknowledgements

This work was partially supported by JST PRESTO (Y.O., JPMJPR16N2 and Y. I., JPMJPR17N2), JST CREST (Y.I., JPMJCR21O1), JSPS-KAKENHI (Y. O., JP22H02148, JP23K23416, JP24K01550, and JP25H00425), and AMED (JP25ym0126819).

Notes and references

1 Y. Osada and J. P. Gong, *Prog. Polym. Sci.*, 1993, **18**, 187.
2 M. M. Caruso, D. A. Davis, Q. Shen, S. A. Odom, N. R. Sottos, S. R. White and J. S. Moore, *Chem. Rev.*, 2009, **109**, 5755.
3 Y. Sagara, S. Yamane, M. Mitani, C. Weder and T. Kato, *Adv. Mater.*, 2016, **28**, 1073.
4 C. Isapour and M. Lattuada, *Adv. Mater.*, 2018, **30**, 1707069.
5 M. I. Khazi, W. Jeong and J. M. Kim, *Adv. Mater.*, 2018, **30**, 1705310.
6 K. Tanaka and Y. Chujo, *Polym. J.*, 2023, **55**, 353.
7 T. Watabe and H. Ohtsuka, *Macromolecules*, 2024, **57**, 425.
8 Y. Oaki and S. Fujii, *Chem. Commun.*, 2024, **60**, 9163.
9 X. Tian, Y. Guo, J. Zhang, O. M. Ivasishin, J. Jia and J. Yan, *Small*, 2024, **20**, 2306952.
10 B. Yoon, T. Oh, Y. J. Chang and J. Suhr, *Small*, 2025, **21**, 2310682.
11 S. Dolui, B. Sahu and S. Banerjee, *Macromol. Chem. Phys.*, 2025, **226**, 2400472.
12 T. Bereau, D. Andrienko and K. Kremer, *APL Mater.*, 2016, **4**, 053101.

13 D. J. Audus and J. J. de Pablo, *ACS Macro Lett.*, 2017, **6**, 1078.
14 J. S. Peerless, N. J. B. Milliken, T. J. Oweida, M. D. Manning and Y. G. Yingling, *Adv. Theory Simul.*, 2019, **2**, 1800129.
15 K. Sattari, Y. Xie and J. Lin, *Soft Mater.*, 2021, **17**, 7607.
16 K. Zhang, X. Gong and Y. Jiang, *Adv. Funct. Mater.*, 2024, **34**, 2315177.
17 K. Hatakeyama-Sato, *Polym. J.*, 2023, **55**, 117.
18 T. Orlova, A. Piven, D. Darmoroz, T. Aliev, T. M. T. A. Razik, A. Boitsev, N. Grafeeva and E. Skorb, *Digital Discovery*, 2023, **2**, 298.
19 K. Wang, H. Shi, T. Li, L. Zhao, H. Zhai, D. Korani and J. Yeo, *Digital Discovery*, 2023, **2**, 1660.
20 C. Yan and G. Li, *Adv. Intell. Syst.*, 2023, **5**, 2200243.
21 T. B. Martin and D. J. Audus, *ACS Polym. Au*, 2023, **3**, 239.
22 W. Ge, R. De Silva, Y. Fan, S. A. Sisson and M. H. Stenzei, *Adv. Mater.*, 2025, **37**, 2413695.
23 S. Okada, S. Peng, W. Spevak and D. Charych, *Acc. Chem. Res.*, 1998, **31**, 229.
24 D. J. Ahn and J. M. Kim, *Acc. Chem. Res.*, 2008, **41**, 805.
25 X. Sun, T. Chen, S. Huang, L. Li and H. Peng, *Chem. Soc. Rev.*, 2010, **39**, 4244.
26 X. Qian and B. Städler, *Chem. Mater.*, 2019, **31**, 1196.
27 Y. Oaki, *Chem. Commun.*, 2020, **56**, 13069.
28 B. Das, S. Jo, J. Zheng, J. Chen and K. Sugihara, *Nanoscale*, 2022, **14**, 1670.
29 Y. Kim, K. Iimura and N. Tamaoki, *Bull. Chem. Soc. Jpn.*, 2024, **97**, uoae034.
30 C. C. Revadekar, A. A. Patil, J. M. Kim and B. J. Park, *J. Photochem. Photobiol., C*, 2025, **63**, 100699.
31 Z. Huo, Q. Deng, T. Fan, G. He, X. Hu, X. Hong, H. Chen, S. Luo, Z. Wang and D. Chen, *Polym. Chem.*, 2017, **8**, 7438.
32 Z. Yu, C. MuYu, H. Xu, J. Zhao and G. Yang, *Polym. Chem.*, 2023, **14**, 2266.
33 A. Thakuri, M. Banerjee and A. Chatterjee, *Chem.–Asian J.*, 2025, **20**, e202500219.
34 S. Dei, M. Matsumoto and A. Matsumoto, *Macromolecules*, 2008, **41**, 2467.
35 S. Ampornpun, S. Montha, G. Tumcharern, V. Vchirawongkwin, M. Sukwattanasinitt and S. Wacharasindhu, *Macromolecules*, 2012, **45**, 9038.
36 J. Seo, C. Kantha, J. F. Joung, S. Park, R. Jelinek and J. M. Kim, *Small*, 2019, **15**, 1901342.
37 B. Hu and P. Wu, *Giant*, 2020, **3**, 100025.
38 B. S. Kim, M. I. Khazi and J. M. Kim, *Macromolecules*, 2021, **54**, 8220.
39 R. Saymung, N. Traiphol and R. Traiphol, *Colloids Surf., A*, 2021, **626**, 120746.
40 S. Baek, J. M. Heo, K. Bae, M. I. Khazi, S. Lee, K. Kim and J. M. Kim, *Langmuir*, 2024, **40**, 18272.
41 N. N. Kadamannil, D. Jang, H. Lee, J. M. Kim and R. Jelinek, *Small Methods*, 2024, **8**, 2301286.
42 J. Zheng, J. Chen, M. Galluzzi, Y. Hou and K. Sugihara, *Nano Lett.*, 2025, **25**, 7307.
43 Y. Takeuchi, H. Imai and Y. Oaki, *J. Mater. Chem. C*, 2025, **13**, 3209.
44 Y. Ishijima, H. Imai and Y. Oaki, *Chem*, 2017, **3**, 509.
45 H. Terada, H. Imai and Y. Oaki, *Adv. Mater.*, 2018, **30**, 1801121.
46 Y. Oaki, Y. Ishijima and H. Imai, *Polym. J.*, 2018, **50**, 319.
47 K. Watanabe, H. Imai and Y. Oaki, *Small*, 2020, **16**, 20045.
48 K. Watanabe, H. Imai and Y. Oaki, *J. Mater. Chem. C*, 2020, **8**, 1265.
49 Y. Mochizuki, H. Imai and Y. Oaki, *ChemPlusChem*, 2021, **86**, 1563.
50 A. Edagawa, S. Matsuda, H. Kawakubo, H. Imai and Y. Oaki, *ACS Appl. Mater. Interfaces*, 2022, **14**, 43792.
51 N. Shioda, J. M. Heo, B. Kim, H. Imai, J. M. Kim and Y. Oaki, *Sens. Diagn.*, 2022, **1**, 163.
52 R. Shibata, S. Matsuda, H. Kawakubo, H. Imai and Y. Oaki, *J. Mater. Chem. B*, 2024, **12**, 10886.
53 S. Curtarolo, G. L. W. Hart, M. B. Nardelli, N. Mingo, S. Sanvito and O. Levy, *Nat. Mater.*, 2013, **12**, 191.
54 K. Rajan, *Annu. Rev. Mater. Res.*, 2015, **45**, 153.
55 K. T. Butler, J. M. Frost, J. M. Skelton, K. L. Svanea and A. Walsh, *Chem. Soc. Rev.*, 2016, **45**, 6138.
56 B. Sanchez-Lengeling and A. Aspuru-Guzik, *Science*, 2018, **361**, 360.
57 A. Agrawal and A. Choudhary, *MRS Commun.*, 2019, **9**, 779.
58 L. Himanen, A. Geurts, A. S. Foster and P. Rinke, *Adv. Sci.*, 2019, **6**, 1900808.
59 Y. Miyake and A. Saeki, *J. Phys. Chem. Lett.*, 2021, **12**, 12391.
60 S. C. Smith, C. S. Horbaczewskyj, T. F. N. Tanner, J. J. Walder and J. S. Fairlamb, *Digital Discovery*, 2024, **3**, 1467.
61 A. D. Sendek, B. Ransom, E. D. Cubuk, L. A. Pellouchoud, J. Nanda and E. J. Reed, *Adv. Energy Mater.*, 2022, **12**, 2200553.
62 Y. Zhang and C. Ling, *npj Comput. Mater.*, 2018, **4**, 25.
63 Y. Liu, B. Guo, X. Zou, Y. Li and S. Shi, *Energy Storage Mater.*, 2020, **31**, 434.
64 B. Dou, Z. Zhu, E. Merkurjev, L. Ke, L. Chen, J. Jian, Y. Zhu, J. Liu, B. Zhang and G. W. Wei, *Chem. Rev.*, 2023, **123**, 8736.
65 P. Xu, X. Ji, M. Li and W. Lu, *npj Comput. Mater.*, 2023, **9**, 42.
66 S. J. Pan and Q. Yang, *IEEE Trans. Knowl. Data Eng.*, 2010, **22**, 1345.
67 A. U. Mahmood, M. M. Ghelardini, J. B. Tracy and Y. G. Yingling, *Chem. Mater.*, 2024, **36**, 9330.
68 Y. Oaki and Y. Igarashi, *Bull. Chem. Soc. Jpn.*, 2021, **94**, 2410.
69 Y. Haraguchi, Y. Igarashi, H. Imai and Y. Oaki, *Digital Discovery*, 2022, **1**, 26.
70 H. Tobita, Y. Namiuchi, T. Komura, H. Imai, K. Obinata, M. Okada, Y. Igarashi and Y. Oaki, *Energy Adv.*, 2023, **2**, 1014.
71 W. Hamada, M. Hishida, R. Sugiura, H. Tobita, H. Imai, Y. Igarashi and Y. Oaki, *J. Mater. Chem. A*, 2024, **12**, 3294.
72 D. Suzuki, H. Minato, Y. Sato, R. Namioka, Y. Igarashi, R. Shibata and Y. Oaki, *Chem. Commun.*, 2024, **60**, 13678.
73 Y. Kitamura, Y. Namiuchi, H. Imai, Y. Igarashi and Y. Oaki, *Nanoscale Adv.*, 2025, **7**, 4620.
74 K. Sakano, Y. Igarashi, H. Imai, S. Miyakawa, T. Saito, Y. Takayanagi, K. Nishiyama and Y. Oaki, *ACS Appl. Energy Mater.*, 2022, **5**, 2074.
75 R. Yamamoto, Y. Igarashi, H. Imai, T. Sakata, S. Miyakawa, S. Yoshizaki, T. Saito and Y. Oaki, *Batteries Supercaps*, 2025, **8**, e202500288.